Fluorescence of Antiaromatic Systems: An Experimental and Theoretical Study of 1,3,5-Tri-*tert*-butylpentalene†

Anna Falchi, Cristina Gellini, and Pier Remigio Salvi*

Laboratorio di Spettroscopia Molecolare, Dipartimento di Chimica, Università di Firenze, Via G. Capponi 9, 50121 Firenze, Italy

Klaus Hafner

Institut fur Organische Chemie der Technische Hochschule, Petersenstrasse 22, D-6100 Darmstadt, Germany

Received: November 21, 1997; In Final Form: April 21, 1998

The fluorescence spectrum of 1,3,5-tri-*tert*-butylpentalene (TTBP), the stable derivative of antiaromatic pentalene, has been measured in solution at room and low temperature in condensed phase. A good correspondence between the first allowed absorption band and the fluorescence spectrum is observed. The fluorescence quantum yield of TTBP 2×10^{-4} M in cyclohexane is estimated to be $\approx 2 \times 10^{-3}$ ($\lambda_{ex} = 313$ nm) at room temperature. At low temperature and exciting at 355 nm, the fluorescence spectrum of TTBP shows appreciable vibronic structure. The fluorescence data have been related to the electronic structure of the parent molecule. MCSCF/CAS calculations for the ground and lowest excited states of pentalene, up to S_4, have been performed in D_{2h} symmetry with 3-21G and 6-31G basis sets including polarization and diffuse orbitals. As a result of the strong interaction between the pairs of states S_0/S_1 and S_2/S_3, the lowest component of each pair distorts from D_{2h} to lower symmetry, giving rise to new equilibrium geometries. According to ab initio calculations, the observed fluorescence is assigned to upper state, $S_3 \rightarrow S_0$, emission.

1. Introduction

Aromaticity and antiaromaticity are widely used concepts to classify structural properties of planar conjugated cyclic molecules[1,2] and the reactivity of cyclic transition states.[3] It is known[1,2] that systems of this type with $(4n + 2)$ π electrons show aromatic stabilization in the ground state while, conversely, those with $4n$ π electrons antiaromatic destabilization. The same counting rule is the factor governing cycloaddition reactivity.[3]

The nature of the cyclic system affects also excited-state properties. However, in contrast with the wealth of data on aromatics,[4−6] equivalent information is not available on antiaromatic molecules. Recently, our group has reported on the vibrational and electronic properties of 1,3,5,7-tetra-*tert*-butyl-*s*-indacene (TTBI)[7,8,9] and 1,3,5-tri-*tert*-butylpentalene (TTBP, see Figure 1),[10] stable derivative[11] of pentalene, the labile parent molecule. The photophysical behavior of TTBI was investigated by another group using femtosecond pulses.[12] A remarkable result on TTBI was the observation of $S_2 \rightarrow S_0$ fluorescence,[8,12] substantially due to the fact that the energy gap $\Delta E(S_2 - S_1)$ is comparable, as in the azulene case,[13,14] to $\Delta E(S_1 - S_0)$. Semiempirical calculations on pentalene[10] indicate that the condition is met also in this case, thus encouraging a similar study on TTBP. In this paper upper state fluorescence of pentalene in condensed phase under various experimental conditions of temperature and in different solvents is investigated.

From the theoretical point of view the observed behavior has been related to the electronic structure of pentalene. Simple arguments based on second-order bond fixation in conjugated molecules[15,16] indicate that the symmetrical, bond-equalized D_{2h} structure of pentalene corresponds to a maximum on the ground-state energy surface and, as a consequence, the molecule distorts to C_{2h} structure with alternating single and double bonds. Semiempirical methods have limited applicability to excited-state surfaces. On the other hand, it has been shown in the case of antiaromatic cyclobutadiene[17] that, determining the multiconfigurational (MC) wave function in the complete-active-space (CAS) scheme of configuration interaction, a good account of surface peculiarities both for the ground and the lowest excited states is obtained. To the best of our knowledge the issue has not been addressed so far in other antiaromatics. In this work similar calculations have been performed on pentalene. According to our ab initio results the fluorescence emission may be assigned as $S_3 \rightarrow S_0$ transition.

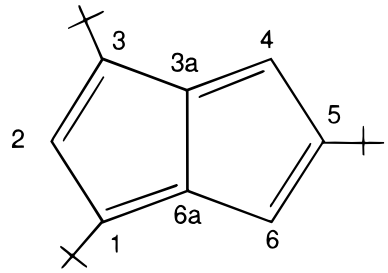

Figure 1. Molecular structure of 1,3,5-tri-*tert*-butylpentalene (TTBP).

2. Experimental Section

The synthesis of TTBP has been described elsewhere.[11] While methyl derivatives of pentalene dimerize even at low temperature,[18,19,20] TTBP has long-term stability at room temperature. Our sample (≈1 g) was conserved under vacuum and

† This work was supported by the Italian Consiglio Nazionale delle Ricerche (CNR) and Ministero dell'Università e della Ricerca Scientifica e Tecnologica (MURST).

S1089-5639(98)00279-5 CCC: $15.00
Published on Web 06/06/1998

in absence of light at −20 °C, and its purity was checked periodically by mass and gas chromatographic analysis.

Fluorescence measurements were taken at room and low temperature. In the first case TTBP solutions in different solvents such as hexane, cyclohexane, methanol, and the isopentane/ether 7:3 mixture (concentration range $10^{-3}-10^{-4}$ M) were used. Also, experiments were carried out both on freshly prepared aerated and deoxygenated cyclohexane solutions. Oxygen was eliminated by repeated thaw-and-freeze processes under relatively high vacuum ($\approx 10^{-4}$ Torr). The UV absorption spectra of these solutions were checked to be coincident with those of past reports.[10,21] Fluorescence spectra were measured with the LS-50 Perkin-Elmer spectrophotofluorimeter, the excitation wavelength varying from 300 to 380 nm. No substantial difference in the fluorescence spectra was found using the two types of sample preparation, apart from a slight increase of the total emission with oxygen-free solutions. Fluorescence excitation spectra of TTBP in cyclohexane and isopentane/ether solutions were also measured with an emission window at 500 nm.

Low-temperature measurements were taken at 77 and 15 K. Highly transparent TTBP solutions in isopentane/ether were prepared in quartz cells under vacuum and then immersed in liquid nitrogen. The TTBP solutions in cyclohexane were deposited on the coldfinger of a closed-cycle He cryostat at 77 K and quickly frozen to 15 K. The samples were excited in pulsed conditions with the third and fourth harmonic of a Nd:YAG laser (355 and 266 nm, respectively). The fluorescence signal, focused on the entrance slit of the monochromator, was detected by a photomultiplier cooled at −20 °C and sent to a boxcar for averaging. The data were finally stored on a personal computer. Each fluorescence spectrum on TTBP, at room and low temperature, was doubled by that of the solvent alone. No interference band was found in the spectral emission range of interest (380−550 nm).

3. Results

3.1. Fluorescence Emission. Exciting at room temperature with $\lambda_{ex} = 313$ nm, the TTBP solutions ($c = 10^{-4}$ M; cyclohexane, *n*-hexane, methanol as solvents) show a broad and unresolved emission with maximum around 25 600 cm^{-1} (≈390 nm) and slowly decreasing intensity up to 18 000 cm^{-1}. The emission profiles are almost independent of the solvent used. The spectra subtracted of the solvent background, much lower under the same experimental conditions than the signal from TTBP and free of emission bands, are shown in Figure 2. The absorption and emission spectra of TTBP in cyclohexane solution are reported in Figure 3. The absorption spectrum has been already discussed on the basis of semiempirical MO calculations.[10,16,21] Common to all calculations is the prediction of a first excited state, S_1, around 10 000 cm^{-1} and of two next, S_2 and S_3, in the range 28 000 to 40 000 cm^{-1}. The $S_0 \rightarrow S_1$ transition is forbidden while $S_0 \rightarrow S_2$ and $S_0 \rightarrow S_3$ are allowed in one-photon spectroscopy with relatively high oscillator strength.[10,21] In our own calculation,[10] which includes the interaction between singly excited configurations (SECI), the three lowest vertical transitions were found at 11 950, 28 380, and 36 070 cm^{-1}. Accordingly, the two lowest absorption bands of TTBP in the ultraviolet region (see Figure 3) were assigned to allowed $S_0 \rightarrow S_2$ and $S_0 \rightarrow S_3$ transitions, respectively. Comparing the emission with the $S_0 \rightarrow S_2$ absorption band, a large Stokes shift may be noted, their respective maxima falling at ≈25 600 and 29 600 cm^{-1} (≈337 nm). The difference is related to the difference between the equilibrium geometries of the ground and the excited states.[22] In fact, according to calculations, S_0 and S_2 have structures belonging to C_{2h} and D_{2h} symmetry, respectively.[10] The average energy, 27 600 cm^{-1}, corresponds approximately to that of the (0−0) transition of the low-temperature absorption spectrum, 27 440 cm^{-1}.[10] This may suggest that the emission arises from the same state responsible for the absorption band. The emission band does not change appreciably with λ_{ex} in the range 300−380 nm, as seen in Figure 4. Only the maximum is moderately red-shifted, increasing λ_{ex}. A weak band, extending up to ≈18 000 cm^{-1}, is observed even exciting at ≈26 300 cm^{-1} (380 nm), i.e., at an energy lower than (0−0). The uncorrected excitation spectrum (not shown), taken with emission window at 500 nm, has a band centered around the same value. Further, anticipating ab initio results of the following subsection, there is also a theoretical indication of one electronic state below the first allowed in this region.

Given these circumstances, it is important to investigate about weak electronic transitions that may be hidden under the wing of the strong $S_0 \rightarrow S_2$ absorption at lower energies. Owing to the excellent optical transparency of glassy matrixes at low temperature, TTBP solutions in isopentane/ether in the concentration range $10^{-3}-10^{-4}$ M were chosen for absorption and emission measurements. The results are collected in Figure 5. The absorption spectrum of the rigid solution ($c = 10^{-4}$ M;

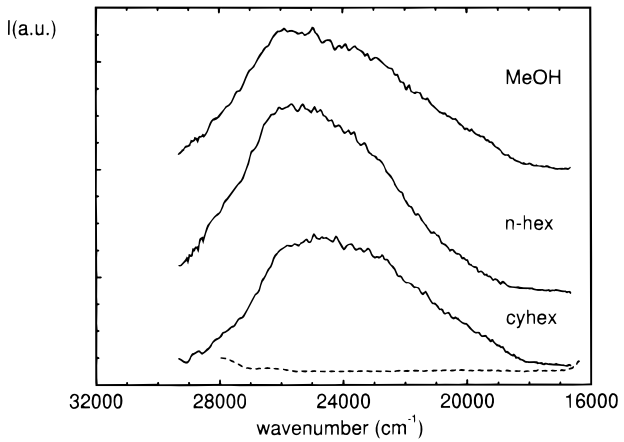

Figure 2. Fluorescence spectra ($\lambda_{ex} = 313$ nm) of TTBP 10^{-4} M in methanol, *n*-hexane, and cyclohexane, from top to bottom, at room temperature. Dashed line, spectrum of solvent cyclohexane under the same experimental conditions. For the sake of clarity, the other two solvent spectra, similar to that of cyclohexane, are not shown.

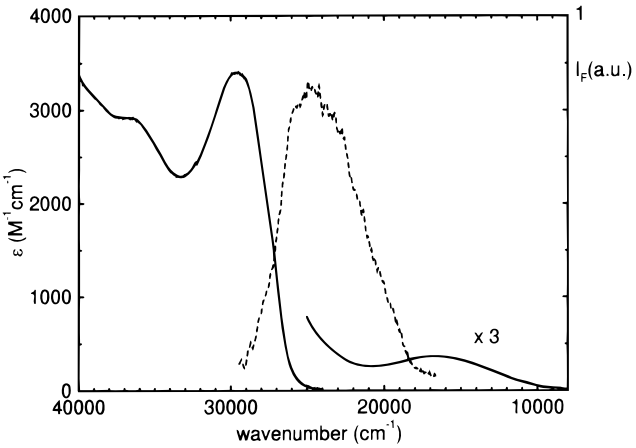

Figure 3. Molar extinction ϵ (cm^{-1} M^{-1}, left; full line) and fluorescence spectrum I_F (right, dashed line; $\lambda_{ex} = 313$ nm, $c = 10^{-4}$ M) of TTBP in cyclohexane solution at room temperature.

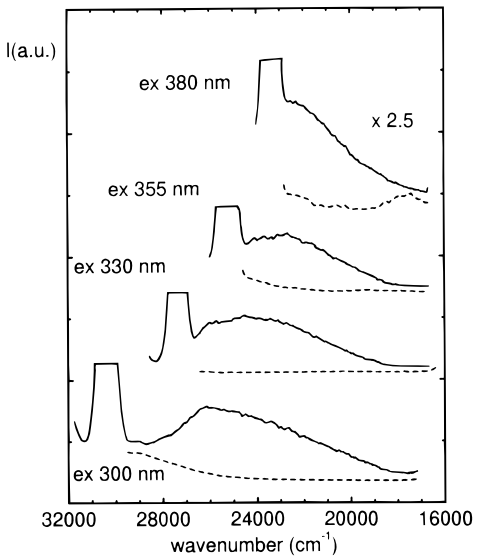

Figure 4. Fluorescence spectra of the deoxygenated TTBP solution 10^{-4} M in cyclohexane at room temperature as a function of the excitation wavelength. The strong band on the high-energy side of each spectrum is the C−H Raman band of the solvent. Dashed lines, solvent spectra under the same experimental conditions.

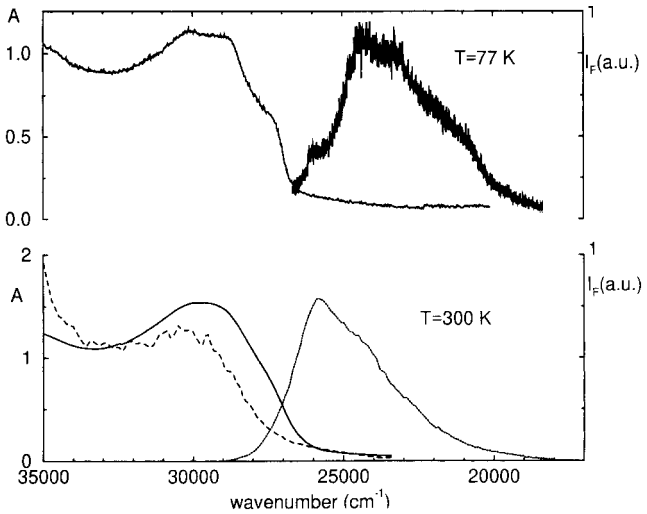

Figure 5. Absorption (A; left) and fluorescence (I_F; right) spectra of TTBP in a isopentane/ether solution (7:3) at room temperature and at 77 K in the region of the first allowed transition. The fluorescence spectra are observed exciting at 355 nm (top) and at 313 nm (bottom), $c = 10^{-3}$ M. In the lower panel, the excitation spectrum is also displayed as a dashed line.

Figure 5, upper) shows at 77 K no evidence of additional band structure to the red of the $S_0 \rightarrow S_2$ absorption band. Further, it has been checked that increasing the TTBP concentration the absorption in the spectral range 370−410 nm shifts uniformly to higher values, without appearance of weak bands. The room temperature excitation spectrum of TTBP (see Figure 5, bottom, emission window 500 nm) matches satisfactorily the absorption spectrum, once account is taken of the variation of the incident intensity and of the beam penetration depth into the solution, as a function of frequency. These results strongly suggest the absence of one electronic state on the low-energy side and in close proximity to S_2.

The emission properties of TTBP have been studied also at low temperature. The fluorescence spectrum of a rigid TTBP solution ($c \approx 10^{-3}$ M, $\lambda_{ex} = 355$ nm, 77 K) is reported in Figure 5, upper. The spectrum is red-shifted with respect to that at

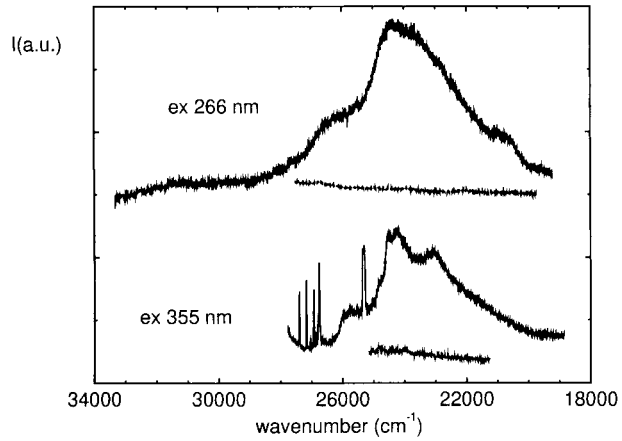

Figure 6. Fluorescence (I_F) spectra of TTBP 10^{-3} M in cyclohexane at 15 K as a function of the excitation wavelength (266 nm, upper; 355 nm, lower). All sharp lines in the 355 nm spectrum are Raman bands of the solvent. The background emission of cyclohexane under the same experimental conditions is also shown for both spectra.

room temperature by ≈1500 cm^{-1}. No shift with the temperature is observed for the absorption spectrum. Changing solvent and lowering the temperature the spectrum becomes more resolved. The spectra of TTBP 10^{-3} M in cyclohexane at 15 K are shown in Figure 6 with 266 and 355 nm excitation wavelengths. With $\lambda_{ex} = 266$ nm the spectrum is still quite diffuse. On the contrary, with 355 nm excitation wavelength the spectrum presents a definite band structure. Vibronic bands are found at 26 000, 25 720, 24 540, 24 280, 23 270, and 23 040 cm^{-1}. The sharp lines, observed in the energy range 27 500−25 000 cm^{-1} and partly overlapping the emission spectrum, are Raman peaks of the solvent. Also in this case the spectrum is shifted to lower energies with respect to that at room temperature.

3.2. Theoretical Results. Although semiempirical MO calculations with singly excited configuration interaction are in good agreement with absorption data on TTBP, the method may not be able to predict or to describe in sufficient detail all the lowest excited states, owing to the neglect of doubly and higher excited configurations. The importance of this group of excitations in antiaromatic cyclobutadiene has been already emphasized.[17] A similar ab initio study is recommended for pentalene. When performing such calculations on antiaromatic molecules, reference is usually made to a geometry without bond alternation.[15−17] In the case of pentalene, this belongs to the D_{2h} group. Structural rearrangements to lower symmetry are recognized by the occurrence of vibrational modes with imaginary frequency when normal modes are calculated for the molecule in the D_{2h} geometry.

Ab initio results were obtained using the 3-21G and 6-31G basis sets, the latter augmented by polarization and polarization + diffuse orbitals on C atoms (6-31G* and 6-31+ G*, respectively). Pentalene has eight π electrons to be distributed over 4π and $4\pi^*$ orbitals whose energies and symmetries are reported in Figure 7 (6-31G basis set, D_{2h} symmetry), together with the schematic representation of the HOMO − 1, HOMO, LUMO, and LUMO + 1 orbitals. The total number of $\pi\pi^*$ excited configurations in the complete active space (CAS) is 1764. From these the multiconfigurational self-consistent-field (MCSCF/CAS) state wave function may be determined. Geometries and vibrational frequencies of the electronic states are then evaluated applying known procedures of optimization[23] and normal mode calculation[24,25] included in the HONDO and GAMESS programs.[26,27]

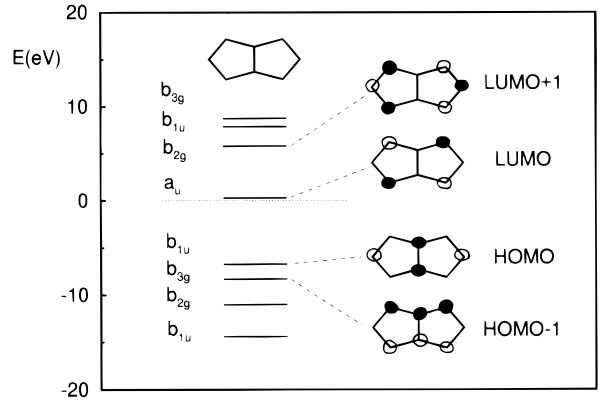

Figure 7. Energy levels (eV) of the eight π orbitals of pentalene in D_{2h} symmetry and schematic representation of the (HOMO − 1), HOMO, LUMO, and (LUMO + 1) orbitals (full and empty circles, positive and negative atomic contributions, respectively; 6-31G results).

Our calculations on pentalene in D_{2h} symmetry show that the ^1A_g state having the largest contribution from the closed-shell configuration, with eight electrons in the four bonding π orbitals, lies at energy higher, whichever the basis set above-mentioned, than the $^1B_{1g}$ state, mostly resulting from the HOMO → LUMO open-shell configuration. The energy difference amounts to 4250 cm^{-1} with the 3-21G and 6-31G and to 3630 cm^{-1} with the 6-31G* basis. Therefore, the ground state of pentalene in D_{2h} symmetry is open-shell, in agreement with previous STO-3G/CI calculations.[28] We recall that also for antiaromatic cyclobutadiene in square D_{4h} geometry the ground state, S_0 (B_{1g}), is open-shell.[17] The S_0 (B_{1g}) and S_1 (A_{1g}) wave functions of cyclobutadiene have been decomposed as combinations of covalent and ionic structures.[17] Following the same procedure and describing the $S_0(B_{1g})$ and $S_1(A_g)$ states of pentalene as ≈(HOMO^1; LUMO^1) and ≈HOMO^2, respectively, with HOMO and LUMO orbitals as in Figure 7, it is easy to express $S_0(B_{1g})$ in terms of only covalent structures with π bonds between adjacent atoms. The $S_1(A_g)$ state is on the contrary represented by ionic and less important covalent forms.

The structures of the ground, S_0 (B_{1g}), and first excited, S_1 (A_g), states are reported in Table 1. Both states have peripheral C−C bond lengths comparable in magnitude, ranging from 1.404 to 1.436 Å, and strongly different interannular bonds, 1.500 Å (S_0) and 1.395 Å (S_1). The structures and energies of higher excited states S_n (n = 2, 3, 4) in D_{2h} symmetry are also reported in Tables 1 and 2, respectively. The structural parameters are not very sensitive to the basis set. On the contrary, the energy of each state is lowered, although not appreciably from 6-31G* to the 6-31+ G* basis. The S_2 state is almost completely determined by the LUMO^2 configurations and therefore of A_g symmetry. The S_3 and S_4 states, of B_{2u} and B_{3u} symmetry, respectively, are mostly represented by singly excited configurations (see Table 3). Also the wave functions of these three states may be decomposed into ionic and valence contributions, starting from their approximate representations. It is seen that while S_2 is predominantly represented by a combination of ionic structures, both covalent and ionic forms contribute to S_3 and S_4.

The vibrational frequencies of S_0 (B_{1g}; D_{2h}) are collected in Table 4. Upon inspection it is seen that the state is not stable with respect to the b_{1g} mode described by adjacent in- and out-of-phase bond stretchings along the main ring. Having this mode imaginary frequency (2310i cm^{-1}, 3-21G; 1766i cm^{-1}, 6-31G; 2726i cm^{-1}, 6-31G*), the D_{2h} geometry is for the S_0 surface a saddle point between equivalent C_{2h} structures with alternating double and single bonds (see Figure 8). The C_{2h} structure corresponds to the global S_0 minimum, all the vibrational frequencies of Table 4 associated to this geometry being real. Bond lengths have similar values with all basis sets. The stabilization energy of S_0 (A_g; C_{2h}) with respect to S_0 (B_{1g}; D_{2h}) is ≈3400 cm^{-1} (3-21G and 6-31G* basis) and ≈2900 cm^{-1} (6-31G basis) and reduces to 2300 cm^{-1} if zero-point vibrational corrections for both states are considered. This value is larger than the estimated experimental energy barrier for TTBP, ≈1400 cm^{-1} (private communication in ref 21). The effect of alkyl

TABLE 1: Optimized C−C Bond Lengths (Å) of Pentalene in the Ground and Lowest Excited Electronic States, According to MCSCF/CAS Calculations with 3-21G, 6-31G*, and 6-31$^+$G* Basis Sets[a]

		$r_{1,6a}$	$r_{1,2}$	$r_{2,3}$	$r_{3,3a}$	$r_{3a,6a}$
$S_0(A_g; C_{2h})$	3-21G	1.351	1.515	1.359	1.479	1.483
	6-31G*	1.352	1.500	1.357	1.472	1.468
	6-31$^+$G*	1.353	1.500	1.359	1.473	1.468
$S_0(B_{1g}; D_{2h})$	3-21G	1.404	1.433			1.509
	6-31G*	1.404	1.426			1.490
$S_1(A_g; D_{2h})$	3-21G	1.436	1.417			1.395
	6-31G*	1.431	1.411			1.390
$S_2(A_1; C_{2v}^b)$	3-21G	1.400	1.482	1.387	1.435	1.479
$S_2(A_g; D_{2h})$	3-21G	1.405	1.427			1.502
	6-31G*	1.402	1.418			1.488
$S_3(B_{2u}; D_{2h})$	3-21G	1.444	1.443			1.413
	6-31G*	1.444	1.434			1.401
$S_4(B_{3u}; D_{2h})$	3-21G	1.440	1.436			1.477
	6-31G*	1.435	1.428			1.459

[a] C atoms are numbered as in Figure 1. [b] C_2 is coincident with the short (y) in-plane axis.

TABLE 2: Electronic Energies (au; MCSCF/CAS Results) of the Ground and Lowest Excited States of Pentalene in D_{2h} Symmetry as a Function of the Basis Set

	E (au)			
state	3-21G	6-31G	6-31G*	6-31$^+$G*
SCF/RHF	−304.599 355	−306.207 840	−306.320 077	−306.332 391
S_0 (A_g; C_{2h})	−304.745 401	−306.352 910	−306.460 816	−306.468 348
S_1 (A_g)	−304.710 749	−306.320 506	−306.428 427	−306.436 880
S_2 (A_g)	−304.615 324	−306.225 429	−306.339 740	−306.349 499
S_3 (B_{2u})	−304.597 012	−306.208 176	−306.316 180	−306.324 498
S_4 (B_{3u})	−304.544 882	−306.156 030	−306.264 636	−306.274 057

[a] Included are also the energies corresponding to the absolute minimum of pentalene in the ground state (C_{2h} symmetry) and the single-determinant restricted HF energies.

TABLE 3: Electronic States of Pentalene in the Optimized D_{2h} and Lower (C_{2h}, C_{2v}) Geometries: Energies with Respect to That of S_0 (C_{2h}) (ΔE; cm^{-1}) and Most Important Configurations Contributing to the MCSCF/CAS State (3-21G Basis Set)

state			ΔE (cm^{-1})	configurations
S_0	C_{2h}	A_g	0	HOMO^2
	D_{2h}	B_{1g}	3 350	HOMO; LUMO
S_1	D_{2h}	A_g	7 660	HOMO^2
S_2	C_{2v}^a	A_1	27 980	HOMO^0; LUMO^2
	D_{2h}	A_g	28 540	HOMO^0; LUMO^2
S_3	D_{2h}	B_{2u}	32 560	(HOMO − 1, HOMO; LUMO^2), (HOMO − 2; LUMO)
S_4	D_{2h}	B_{3u}	44 000	(HOMO − 1; LUMO), (HOMO; LUMO + 1)

[a] C_2 is coincident with the short (y) in-plane axis.

TABLE 4: Normal Frequencies (cm^{-1}) of Pentalene in the S_0 State (MC-SCF/CAS Results; 3-21G, 6-31G, and 6-31G* Basis Sets)[a]

	S_0 (C_{2h})				S_0 (D_{2h})		
	3-21G	6-31G	6-31G*		3-21G	6-31G	6-31G*
a_g	675	699	689	a_g	720	732	715
	797	792	771		904	873	928
	859	907	911		1076	1108	1100
	948	1017	1029		1383	1482	1453
	1204	1206	1195		1517	1557	1538
	1259	1288	1282		3382	3401	3381
	1395	1440	1450		3404	3434	3400
	1485	1492	1498				
	1606	1627	1648	b_{1g}	831	932	805
	1714	1744	1748		1264	1294	1244
	3401	3396	3394		1313	1306	1309
	3422	3421	3410		1556	1573	1592
	3433	3435	3430		2310*i*	1766*i*	2726*i*
					3401	3508	3400
b_g	555	557	539	b_{2g}	538	541	524
	681	681	654		753	747	726
	781	778	749		904	901	846
	884	883	842				
	954	945	892	b_{3g}	721	720	707
					837	829	768
a_u	188	191	178	a_u	304	303	297
	309	311	307		799	790	737
	538	538	515				
	739	736	700	b_{1u}	228	226	221
	880	876	831		559	560	545
	952	944	887		774	768	734
					913	911	852
b_u	472	492	491	b_{2u}	500	507	492
	918	937	913		1106	1121	1110
	973	1019	1026		1174	1189	1195
	1085	1123	1122		1417	1429	1416
	1216	1225	1211		1509	1533	1529
	1380	1383	1373		3402	3477	3402
	1484	1484	1482				
	1570	1591	1609	b_{3u}	954	911	915
	1689	1711	1718		1041	1091	1066
	3405	3402	3396		1372	1350	1375
	3427	3430	3426		1494	1514	1526
	3467	3470	3456		3382	3438	3381
					3412	3622	3408

[a] Symmetry species are given with reference to *x* as long, *y* as short in-plane, and *z* as normal to the plane axis for both D_{2h} and C_{2h} groups.

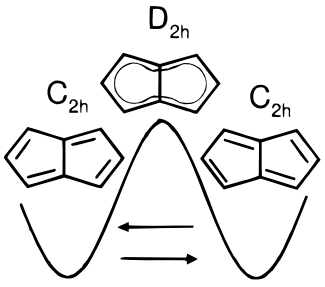

Figure 8. Valence isomerization of pentalene.

substitution on the parent molecule, not taken into account in the present calculation, would reasonably decrease the calculated value.

Normal mode calculations on S_2 in D_{2h} symmetry indicate that this state has one b_{2u} imaginary frequency (1262*i* cm^{-1}, 3-21G; 1225*i* cm^{-1}, 6-31G; 997*i* cm^{-1}, 6-31G*). Therefore, according to calculations results, a distortion from D_{2h} to C_{2v} symmetry is induced in S_2 (A_g; D_{2h}) by coupling with S_3 (B_{2u}; D_{2h}), giving rise to an equilibrium geometry stretched along the short in-plane axis. The C_{2v} structure (see Table 1) corresponds to a minimum on the potential energy surface of S_2; it was checked that all the vibrational frequencies are real. Schematic potential energy curves describing our theoretical results for S_0 and the first three excited states of pentalene are sketched in Figure 9, while all theoretical results with the 3-21G basis set are collected in Table 3.

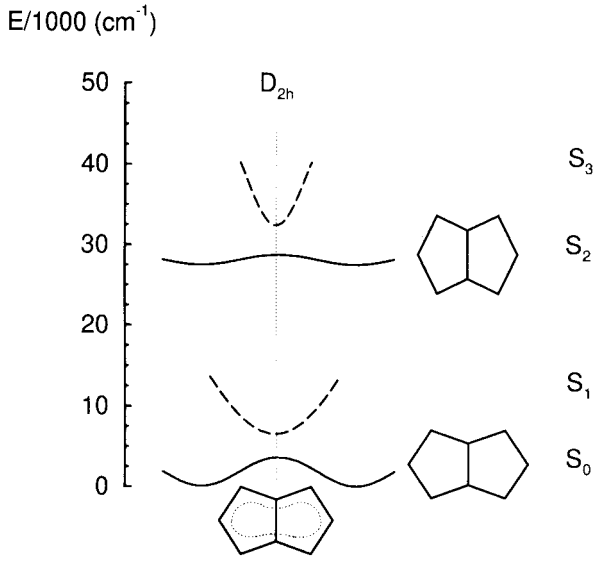

Figure 9. Schematic potential energy curves of the first four states of pentalene as a function of the displacement from D_{2h} geometry (vertical dotted line). Full lines: results from 3-21G MCSCF/CAS calculations. Dashed lines: estimated behavior of the potential energy. Displaced potential minima correspond to the equilibrium structures on the right (exaggerated view, for the sake of clarity).

4. Discussion

When ab initio results on pentalene are compared with those obtained from semiempirical calculations and with experimental data,[10,21] two points must be considered. First, the ab initio calculation indicates as second excited-state one with predominant contribution from the $LUMO^2$ configuration. This is plausible since, as it may be seen from Figure 7, the LUMO orbital is substantially nonbonding and approximately equidistant from the HOMO and LUMO + 1 orbitals. This makes the double $HOMO^2 \rightarrow LUMO^2$ excitation to be of energy comparable to lowest singles. The result is also in qualitative agreement with MCSCF/CAS calculations on excited states of cyclobutadiene.[17] The highest occupied π MO's of cyclobutadiene in square geometry are doubly degenerate. The degeneracy is lifted under rectangular or rhomboidal deformation, the symmetry being lowered from D_{4h} to D_{2h}. In the distorted geometry the three lowest singlets are approximately represented by ($HOMO^1$; $LUMO^1$), $HOMO^2$, and $LUMO^2$ configurations,[17] respectively, in close analogy with the results on pentalene. The S_2 (A_g) $\approx$ $LUMO^2$ state is therefore common to both antiaromatic systems. This state is obviously missing in semiempirical SECI calculations.[10,21] As a consequence, the lowest excited states with allowed activity are S_3 and S_4 in ab initio and S_2 and S_3 in semiempirical calculations.

On the other hand, it should be noted, when comparison is made with experiment, that the observed band maxima of the two lowest allowed transitions are in remarkably good agreement with semiempirical $S_0 \rightarrow S_2$ and $S_0 \rightarrow S_3$ vertical energies.[10,21] On the contrary, there are discrepancies with the ab initio values of Tables 2 and 3, $\approx$0.5 eV for $S_0 \rightarrow S_3$ and $\approx$1 eV for $S_0 \rightarrow S_4$, roughly independent of the basis set. In addition, as observed in the last section, no band structure is found in the

energy range 22000−27000 cm^{-1}, where the $S_2(A_g)$ is theoretically expected. It appears that, while ordering of the lowest excited states of pentalene, summarized in Figure 9, is well-established on an ab initio basis, the calculated energies may be affected by relatively large uncertainties. Tentatively, the deficiency has been related to the partial ionic character of the lowest excited states of pentalene. Difficulties in the MCSCF/CAS approach to valence $\pi\pi^*$ states with predominant ionic character, for instance, the $S_2(B_{1u})$ and $S_3(E_{1u})$ states of benzene, have been already reported, with energy differences from experimental results as large as 1.4 eV.[29−31].

Having these considerations in mind, the proposed assignment for the observed emission is, on the basis of the ab initio results, to the $S_3 \rightarrow S_0$ transition. There is a good correspondence between absorption and emission spectra, with vibronic intervals from the respective origin bands of ≈1400 and 2600 cm^{-1} (see Figure 5, upper). The fluorescence spectrum is shifted to the red when the temperature is decreased to 77 K, while the absorption spectrum remains unaffected. As a consequence, the absorption and emission origin bands do not coincide at low temperature. Anomalous Stokes shifts due to the different intermolecular interactions of the solute molecule with the solvent in the ground and excited states are known.[22] In our case, however, a common origin is observed comparing the absorption and emission spectra at room temperature. As a possible alternative hypothesis, it should be recalled that the D_{2h} equilibrium geometry is for the ground state a saddle point ≈1400 cm^{-1} higher in energy than the bond alternating C_{2h} structure (private communication in ref 21). A $S_3 \rightarrow S_0$ transition with the TTBP molecule "frozen" in D_{2h} symmetry, due to pulsed excitation at low temperature, would fit the experimental result. It should be also noted in Figure 6 the dependence of the low temperature fluorescence spectrum on the excitation energy. This occurs when narrow band laser sources are used to excite selectively a portion of molecules among those determining the inhomogeneous band profile.[32] Site-selected spectroscopy has been extensively applied in fluorescence studies.[33−36] A moderate effect is evident in our spectra changing the excitation from 266 to 355 nm. At the excitation energy $(0-0)(S_0 - S_3) + 730$ cm^{-1} (i.e., 355 nm), molecules belonging to few inhomogeneously broadened vibronic levels are excited, thus enhancing effectively the spectral resolution. Exciting in a region of high vibronic density (for instance, with the 266 nm laser beam), selectivity is lost and the spectrum becomes more diffuse.[32]

The radiative rate constant $k_r(S_3)$ of the $S_3 \rightarrow S_0$ emission of TTBP is obtained with good approximation from experimental data, i.e., oscillator strength f and wavenumber ν_{max} of the absorption maximum, using the relation $k_r \approx f\,\nu_{max}^2$.[22,37] From $f = 0.11$ and $\nu_{max} \approx 30\,000$ cm^{-1},[10] $k_r(S_3)$ results ≈ 10^8 s^{-1}. The fluorescence quantum yield $\eta(S_3)$ of a TTBP solution 2×10^{-4} M in cyclohexane has been estimated ≈2×10^{-3} in this work, exciting at 313 nm and by comparison with the fluorescence yield of pyrene.[5] The corresponding values for the $S_2 \rightarrow S_0$ emission of TTBI are $k_r(S_2) = 10^8$ s^{-1} and $\eta(S_2) = 9 \times 10^{-5}$.[12] The fluorescence rate constant of TTBI, $k_f(S_2) = 4 \times 10^{11}$ s^{-1}, measured directly by means of femtosecond transient absorption spectroscopy,[12] is consistent with that obtained through the relation $k_f(S_2) = k_r(S_2)/\eta(S_2)$. Using the same relation for TTBP a $k_f(S_3)$ value of ≈5×10^{10} s^{-1} is obtained. It was also found for TTBI[12] that the S_2 and S_1 relaxation rates are comparable, 4×10^{11} s^{-1} and 5.6×10^{10} s^{-1}, respectively, and that the $S_2 \rightarrow S_0$ relaxation dynamics does not involve as intermediate step the $S_2 \rightarrow S_1$ internal conversion (IC). A direct $S_2 \rightarrow S_0$ decay was assumed. As to TTBP, only qualitative considerations may be advanced about the origin of the $S_3 \rightarrow S_0$ fluorescence with present data. In principle, the $S_3 \rightarrow S_2$ internal conversion should be first discussed as a possible source of relaxation. The process depends essentially (i) on the overlap or Franck−Condon factor between vibrational wave functions of S_3 and S_2 and, therefore, on the energy difference between the two states and (ii) on their electronic coupling due to terms of the molecular Hamiltonian nondiagonal in the Born−Oppenheimer approximation.[38] The calculated energy gap, $\Delta E(S_3-S_2) \approx 4000$ cm^{-1}, is too small to slow the internal conversion process. However, difficulties in the calculation of excited-state energies have been already noted. Experimentally, the gap is larger, since no bands are observed between $(0-0)(S_3 - S_0)$, 27 440 cm^{-1}, and 20 000 cm^{-1} (see Figure 5). A second plausible reason of the $S_3 \rightarrow S_0$ fluorescence is related to the molecular geometries of the ground and excited states. In fact, in the case of TTBI the $S_2 \rightarrow S_0$ emission was favored by the electronic S_2-S_0 coupling larger than that between S_2 and S_1, owing to the fact that S_2 and S_1 have similar structures while S_2 and S_0 are strongly different.[12] It may be seen from Table 1 that the S_3 geometry of pentalene has a similar behavior with respect to those of S_2 and S_0, thus suggesting that a combination of electronic and structural factors may be responsible for the observed fluorescence.

5. Conclusions

In this paper the emission properties of antiaromatic TTBP under various experimental conditions have been studied. The $S_3 \rightarrow S_0$ fluorescence emission has been observed exciting in the UV region. Upper state, $S_2 \rightarrow S_0$, fluorescence under low-intensity excitation has been first reported for azulene[13,14] and later for other molecular systems.[39,40] In the TTBP case the anomalous fluorescence may be attributed to several reasons, including the relatively large radiative constant of S_3 and electronic and geometry-related factors. Our assignment is supported by extensive MCSCF/CAS calculations of ground- and excited-state energies and wave functions.

Upper state, i.e., $S_2 \rightarrow S_0$, fluorescence has been reported also for antiaromatic TTBI.[12,8] It would be tempting to assume that the anti-Kasha fluorescence emission is a common property of several antiaromatic systems, related to the position of the LUMO orbital, almost nonbonding and equidistant from HOMO and (LUMO + 1). This may favor the location of the lowest states, S_1 and S_2, closer to S_0 than to S_3. It would be of interest, following this hypothesis, to investigate about fluorescence processes, $S_n \rightarrow S_0$, in other simple antiaromatic molecules such as cyclobutadiene and heptalene.

References and Notes

(1) Garratt, P. J. *Aromaticity;* John Wiley and Sons: New York, 1986.
(2) Minkin, V. I.; Glukhovtsev, M. N.; Simkin, B. Y. *Aromaticity and Antiaromaticity;* John Wiley and Sons: New York, 1994.
(3) Pross, A. *Theoretical and physical principles of organic reactivity;* John Wiley and Sons: New York, 1995.
(4) Herzberg, G. *Electronic spectra of polyatomic molecules;* Van Nostrand: New York, 1975.
(5) Berlman, I. D. *Handbook of Fluorescence Spectra of Aromatic Molecules;* Academic Press: New York, 1971.
(6) Ziegler, L. D.; Hudson, B. S.; *Excited States*; Lim, E. C., Ed., Academic Press: New York, 1982.
(7) Gellini, C.; Cardini, G.; Salvi, P.; Marconi, G.; Hafner, K. *J. Phys. Chem.* **1993**, *97*, 1286−1293.
(8) Gellini, C.; Salvi, P. R.; Hafner, K. *J. Phys. Chem.* **1993**, *97*, 8152.
(9) Gellini, C.; Angeloni, L.; Salvi, P. R.; Marconi, G. *J. Phys. Chem.* **1995**, *99*, 85.
(10) Falchi, A.; Gellini, C.; Salvi, P. R.; Hafner, K. *J. Phys. Chem.* **1995**, *99*, 14659.

(11) Hafner, K.; Suss, H. U. *Angew. Chem., Int. Ed. Engl.* **1973**, *12*, 575.
(12) Klann, R.; Bäuerle, R. J.; Laermer, F.; Elsaesser, T.; Niemeyer, M.; W. Lüttke. *Chem. Phys. Lett.* **1990**, *169*, 172.
(13) Beer, M.; Longuet-Higgins, H. C. *J. Chem. Phys.* **1955**, *23*, 1390.
(14) Murata, S.; Iwanaga, C.; Toda, I.; Kokubun, H. *Chem. Phys. Lett.* **1972**, *15*, 152.
(15) Binsch, G.; Heilbronner, E.; Murrell, J. N. *Mol. Phys.* **1966**, *11*, 305.
(16) Nakajima, T. *Top. Curr. Chem.* **1972**, *32*, 1.
(17) Nakamura, K.; Osamura, Y.; Iwata, S. *Chem. Phys.* **1989**, *136*, 67.
(18) Hafner, K.; R. Dönges.; Goedecke, E.; Kaiser, R. *Angew. Chem., Int. Ed. Engl.* **1973**, *85*, 363.
(19) Bloch, R.; Marty, R. A.; de Mayo, P. *J. Am. Chem. Soc.* **1971**, *93*, 3071.
(20) Bloch, R.; Marty, R. A.; de Mayo, P. *Bull. Soc. Chim. Fr.* **1972**, page 2031.
(21) Bischof, P.; Gleiter, R.; Hafner, K.; Knauer, K. H.; Spanget-Larsen, J.; Suss, H. U. *Chem. Ber.* **1978**, *111*, 932.
(22) Klessinger, M.; Michl, J. *Excited states and photochemistry of organic molecules;* VCH Publishers: New York, 1994.
(23) Baker, J. *J. Comput. Chem.* **1986**, *7*, 385.
(24) Gwinn, W. D. *J. Chem. Phys.* **1971**, *55*, 477.
(25) Pulay, P.; Fogarasi, G.; Boggs, J. E. *J. Am. Chem. Soc.* **1979**, *101*, 2550.
(26) Dupuis, M.; Farazdel, A. *HONDO-8 in MOTECC-91;* Clementi, E., Ed.; ESCOM: Leiden, 1991.
(27) Dupuis, M.; Spangler, D.; Wendoloski, J. J. *NRCC Software Catalog, vol.1, program n.QG01, GAMESS;* University of California, 1980.
(28) Kataoka, M.; Koseki, S.; Nakajima, T.; Iida, K. *Nouv. J. Chim.* **1985**, *9*, 135.
(29) Hay, P. J.; Shavitt, I. *J. Chem. Phys.* **1974**, *60*, 2865.
(30) Roos, B. O.; Taylor, P. R.; Siegbahn, P. E. *Chem. Phys.* **1980**, *48*, 157.
(31) Matos, J. M. O.; Roos, B. O.; Malmqvist, P.-A. *J. Chem. Phys.* **1987**, *86*, 1458.
(32) Personov, R. I. In *Spectroscopy and excitation dynamics of condensed molecular crystals;* Agranovich, V. M., Hochstrasser, R. M., Eds.; North-Holland: Amsterdam, 1983; p 555.
(33) Personov, R.; Al'shits, E.; Bykovskaya, L. *Opt. Commun.* **1972**, *6*, 169.
(34) Personov, R. I.; Al'shits, E. I. *Chem. Phys. Lett.* **1975**, *33*, 85.
(35) Bykovskaya, L. A.; Personov, R. I.; Romanovskii, Y. V. *Anal. Chim. Acta* **1981**, *125*, 1.
(36) Catani, L.; Gellini, C.; Salvi, P. R. *J. Phys. Chem.* **1998**, *102*, 1945.
(37) Turro, N. J. *Modern Molecular Photochemistry;* University Science Book, Mill Valley, CA 1991.
(38) Henry, B. R.; Siebrand, W. In *Organic Molecular Photophysics*; John Wiley and Sons: New York, 1973; Vol. I.
(39) Huber, J. R.; Mahaney, M. *Chem. Phys. Lett.* **1975**, *30*, 410.
(40) Hui, M. H.; Mayo, P. D.; Suau, R.; Ware, W. R. *Chem. Phys. Lett.* **1975**, *31*, 257.